Advances in Applied Mathematics and Mechanics
Adv. Appl. Math. Mech., Vol. **2**, No. 3, pp. 333-354

DOI: 10.4208/aamm.09-m0959
June 2010

Accurate 8-Node Hybrid Hexahedral Elements with Energy-Compatible Stress Modes

Shiquan Zhang[1] and Xiaoping Xie[1,*]

[1] *School of Mathematics, Sichuan University, Chengdu 610064, China*

Received 1 July 2009; Accepted (in revised version) 7 November 2009
Available online 25 March 2010

Abstract. In this paper, an energy-compatibility condition is used for stress optimization in the derivation of new accurate 8-node hexahedral elements for three-dimensional elasticity. Equivalence of the proposed hybrid method to an enhanced strains method is established, which makes it easy to extend the method to general nonlinear problems. Numerical tests show that the resultant elements possess high accuracy at coarse meshes, are insensitive to mesh distortions and free from volume locking in the analysis of beams, plates and shells.

AMS subject classifications: 65N12, 65N30.

Key words: Finite element, hybrid stress method, Hellinger-Reissner principle, locking.

1 Introduction

Due to their computational efficiency and simple geometry, low-order hexahedral and tetrahedral elements are the most exploited in the 3D analysis of general solid and structural mechanics problems. However, conventional low-order elements yield poor results at coarse meshes for problems with bending, and suffer from locking at the nearly incompressible limit. To improve their performance, several kinds of enhanced stress/ strain methods have been developed based on generalized variational principles. The first kind is the assumed stress method based on the Hellinger-Reissner principle, where the displacement and stress fields are the assumed independent variables. Representative of this approach for 2D and 3D analysis are the works [1–25]. The second is the enhanced strain method based on the Hu-Washizu principle, where the displacement, stress and strain fields are the assumed independent variables. In this direction, there are a number of works, e.g., [26–55]. The combined hybrid method is the third kind of enhanced stress method which includes displacement and stress

*Corresponding author.
Email: guquan811119@163.com (S. Zhang), xpxie@scu.edu.cn(X. Xie)

variables. It is based on weighted combination of the Hellinger-Reissner functional and its dual, the primal hybrid functional. For the related work one can see [56–59].

Among these methods, the 3-field enhanced strain approach is more attractive in non-linear analysis, since the Hu-Washizu functional is formulated in terms of the strain energy function. But from a practical viewpoint, the 2-field assumed stress approach is more computationally efficient, which makes it more popular. For this method, the choice of stress mode is key to the construction of high performance elements. To improve the performance of the 8-node isoparametric trilinear hexahedron element $H8$ by the assumed stress approach, Spilker and Singh [11] derived an isoparametric quadratic displacement element. However, as the chosen stress field must satisfy equilibrium, then the interpolation must be given in terms of Cartesian co-ordinates. Furthermore, it is necessary to perform inversion operations on a fairly high-order matrix in computing the stiffness matrix. On the other hand, Pian and Tong [2] used isoparametric interpolation and relaxed the equilibrium conditions by introducing Wilson internal displacements parameters [60]. In this way, they constructed a 8-node hybrid stress hexahedral element $PT18\beta$ in which the stress interpolation functions are similar to those given by Loikkanen and Irons [61]. By using admissible matrix formulation, Sze [15–17] improved $PT18\beta$ to obtain better performance for thin plates and shells.

In [23, 25], Xie and Zhou showed that for 2D analysis, fulfillment of the following energy-compatibility (or energy-orthogonality) condition

$$\int_K \boldsymbol{\tau} \cdot \epsilon(\mathbf{v}_I) d\Omega = 0, \qquad \forall \boldsymbol{\tau}, \quad \text{and} \quad \forall \mathbf{v}_I,$$

can lead to optimal stress mode and robust hybrid stress element, where K denotes an arbitrary quadrilateral, $\boldsymbol{\tau}$ the assumed stresses, $\mathbf{v}_I$ the Wilson internal displacements, $\mathbf{n}$ the unit outer normal vector along ∂K. Following the same idea, in this contribution we will use the above stress optimization condition to derive new 8-node hybrid stress hexahedral elements for the analysis of solid mechanical problems, including beams, plates and shells. Following the idea of Piltner [33, 34], we will also discuss the equivalence of the new method to an enhanced strains method.

2 Mixed/ hybrid finite element formulations

Consider the linear elasticity problem

$$\begin{cases} -\mathbf{div}\sigma = \mathbf{f}, & \sigma = D\varepsilon(\mathbf{u}), & \text{in} \quad \Omega, \\ \sigma \cdot \mathbf{n}|_{\Gamma_1} = T, & \mathbf{u}|_{\Gamma_0} = 0, & \text{on} \quad \partial\Omega = \Gamma_1 \bigcup \Gamma_0, \end{cases} \tag{2.1}$$

where $\Omega \subset \Re^3$ is a bounded open set, $\mathbf{u}$ represent the displacements, σ the stress tensor, $\epsilon(\mathbf{u}) = (\nabla\mathbf{u} + \nabla^T\mathbf{u})/2$ the strains, $\mathbf{D}$ the elasticity module matrix, $\mathbf{f}$ the prescribed body forces, $\mathbf{T}$ the prescribed surface traction on Neumman boundary Γ_1.

When incompatible displacements are used in the construction of hybrid stress finite element method, the Hellinger-Reissner variational principle reads as

$$\Pi(\boldsymbol{\sigma}^h, \mathbf{u}^h) = \inf_{\mathbf{v}\in\mathbf{u}^h} \sup_{\boldsymbol{\tau}\in\mathbf{v}^h} \Pi(\tau, \mathbf{v}), \tag{2.2}$$

where the energy functional

$$\Pi(\boldsymbol{\tau}, \mathbf{v}) = \sum_K \Big[-\frac{1}{2}\int_K \boldsymbol{\tau}\cdot\mathbf{D}^{-1}\boldsymbol{\tau} d\Omega + \int_K \boldsymbol{\tau}\cdot\epsilon(\mathbf{v}) d\Omega - \oint_{\Gamma_1\cap\partial K} \mathbf{T}\cdot\mathbf{v}_c ds - \oint_{\partial K} \boldsymbol{\tau}\mathbf{n}\cdot\mathbf{v}_I ds - \int_K \mathbf{f}\cdot\mathbf{v} d\Omega\Big],$$

displacements $\mathbf{v} = \mathbf{v}_c + \mathbf{v}_I$ with $\mathbf{v}_c$ the compatible element displacements and $\mathbf{v}_I$ the incompatible internal displacements, $\boldsymbol{\tau}$ are piecewise-independent stresses,

$$\mathbf{U^h} = \mathbf{U_c^h} \bigoplus \mathbf{U_I^h}, \quad \text{and} \quad \mathbf{V^h} \subset \mathbf{V} := \prod_{\mathbf{K}\in\mathbf{T_h}} \mathbf{H}(\mathrm{div}; \mathbf{K}),$$

denote respectively the finite dimensional approximation subspaces for displacements and stresses such that

$$\mathbf{U_c^h} \subset \mathbf{U_c} := \big\{\mathbf{v} \in H^1(\Omega)^3;\ \mathbf{v}|_{\Gamma_0} = 0\big\},$$
$$\mathbf{U_I^h}\big|_K := \mathrm{span}\big\{\text{incompatible internal bubble displacements}\big\},$$

with $T_h = \bigcup\{K\}$ a given hexahedral mesh subdivision, $H^1(\Omega)$ the usual Sobolev space, $L^2(\Omega)$ the square-integrable function space,

$$\mathbf{H}(\mathrm{div}; K) = \Big\{\tau = (\boldsymbol{\tau}_{11}, \boldsymbol{\tau}_{22}, \boldsymbol{\tau}_{33}, \boldsymbol{\sigma}_{12}, \boldsymbol{\tau}_{13}, \boldsymbol{\tau}_{23})^T \in L^2(\Omega)^6;\ \mathbf{div}\boldsymbol{\tau} \in L^2(\Omega)^3\Big\},$$

where

$$\mathbf{div}\boldsymbol{\tau} = \Big(\frac{\partial\boldsymbol{\tau}_{11}}{\partial x} + \frac{\partial\boldsymbol{\tau}_{12}}{\partial y} + \frac{\partial\boldsymbol{\tau}_{13}}{\partial z},\ \frac{\partial\boldsymbol{\tau}_{12}}{\partial x} + \frac{\partial\boldsymbol{\tau}_{22}}{\partial y} + \frac{\partial\boldsymbol{\tau}_{23}}{\partial z},\ \frac{\partial\boldsymbol{\tau}_{13}}{\partial x} + \frac{\partial\boldsymbol{\tau}_{23}}{\partial y} + \frac{\partial\boldsymbol{\tau}_{33}}{\partial z}\Big)^T.$$

2.1 Element geometry and stress modes

Let K be an arbitrary hexahedron with eight vertices $P_i(x_i, y_i, z_i)(i = 1, ..., 8)$. The isoparametric mapping

$$\mathbf{F_K} : \widehat{K} = [-1, 1]^3 \to K,$$

is given by

$$\begin{pmatrix} x \\ y \\ z \end{pmatrix} = F_K(\xi, \eta, \zeta) = \frac{1}{8}\sum_{i=1}^{8} N_i \begin{pmatrix} x_i \\ y_i \\ z_i \end{pmatrix},$$

where ξ, η and ζ are the isoparametric coordinates,

$$N_i = (1+\xi_i\xi)(1+\eta_i\eta)(1+\zeta_i\zeta),$$

$$\begin{pmatrix} \xi_1 & \xi_2 & \xi_3 & \xi_4 & \xi_5 & \xi_6 & \xi_7 & \xi_8 \\ \eta_1 & \eta_2 & \eta_3 & \eta_4 & \eta_5 & \eta_6 & \eta_7 & \eta_8 \\ \zeta_1 & \zeta_2 & \zeta_3 & \zeta_4 & \zeta_5 & \zeta_6 & \zeta_7 & \zeta_8 \end{pmatrix} = \begin{pmatrix} -1 & 1 & 1 & -1 & -1 & 1 & 1 & -1 \\ -1 & -1 & 1 & 1 & -1 & -1 & 1 & 1 \\ -1 & -1 & -1 & -1 & 1 & 1 & 1 & 1 \end{pmatrix}.$$

We denote the element geometric parameters as follows

$$\begin{pmatrix} a_1 & b_1 & c_1 \\ a_2 & b_2 & c_2 \\ a_3 & b_3 & c_3 \\ a_4 & b_4 & c_4 \\ a_5 & b_5 & c_5 \\ a_6 & b_6 & c_6 \\ a_7 & b_7 & c_7 \end{pmatrix} = \frac{1}{8} \begin{pmatrix} -1 & 1 & 1 & -1 & -1 & 1 & 1 & -1 \\ -1 & -1 & 1 & 1 & -1 & -1 & 1 & 1 \\ -1 & -1 & -1 & -1 & 1 & 1 & 1 & 1 \\ 1 & -1 & 1 & -1 & 1 & -1 & 1 & -1 \\ 1 & -1 & -1 & 1 & -1 & 1 & 1 & -1 \\ 1 & 1 & -1 & -1 & -1 & -1 & 1 & 1 \\ -1 & 1 & -1 & 1 & 1 & -1 & 1 & -1 \end{pmatrix} \begin{pmatrix} x_1 & y_1 & z_1 \\ x_2 & y_2 & z_2 \\ x_3 & y_3 & z_3 \\ x_4 & y_4 & z_4 \\ x_5 & y_5 & z_5 \\ x_6 & y_6 & z_6 \\ x_7 & y_7 & z_7 \\ x_8 & y_8 & z_8 \end{pmatrix}.$$

Then the Jacobian of the co-ordinate transformation F_K is

$$\begin{aligned} [J] &= \begin{pmatrix} \frac{\partial x}{\partial \xi} & \frac{\partial y}{\partial \xi} & \frac{\partial z}{\partial \xi} \\ \frac{\partial x}{\partial \eta} & \frac{\partial y}{\partial \eta} & \frac{\partial z}{\partial \eta} \\ \frac{\partial x}{\partial \zeta} & \frac{\partial y}{\partial \zeta} & \frac{\partial z}{\partial \zeta} \end{pmatrix} \\ &= \begin{pmatrix} a_1 + a_4\eta + a_5\zeta + a_7\eta\zeta & b_1 + b_4\eta + b_5\zeta + b_7\eta\zeta & c_1 + c_4\eta + c_5\zeta + c_7\eta\zeta \\ a_2 + a_4\xi + a_6\zeta + a_7\xi\zeta & b_2 + b_4\xi + b_6\zeta + b_7\xi\zeta & c_2 + c_4\xi + c_6\zeta + c_7\xi\zeta \\ a_3 + a_5\xi + a_6\eta + a_7\xi\eta & b_3 + b_5\xi + b_6\eta + b_7\xi\eta & c_3 + c_5\xi + c_6\eta + c_7\xi\eta \end{pmatrix}. \end{aligned}$$

Let

$$\begin{aligned} \mathbf{U}_1^h := \Big\{ & \mathbf{v}_c \in \mathbf{U}_c \cap C^0(\overline{\Omega}); \\ & \mathbf{v}_c|_K \in \text{span}\{1, \xi, \eta, \zeta, \xi\eta, \eta\zeta, \zeta\xi, \xi\eta\zeta\}^3 \circ F_K^{-1}, \quad \forall K \in T_h \Big\}, \end{aligned}$$

be the compatible isoparametric trilinear displacement subspace, i.e., for $\mathbf{v}_c \in \mathbf{U}_1^h$,

$$\begin{aligned} \mathbf{v}_c|_K &= \Big[N_1\mathbf{I}_3 \quad N_2\mathbf{I}_3 \quad N_3\mathbf{I}_3 \quad N_4\mathbf{I}_3 \quad N_5\mathbf{I}_3 \quad N_6\mathbf{I}_3 \quad N_7\mathbf{I}_3 \quad N_8\mathbf{I}_3 \Big] q_c^{(\mathbf{v})} \\ &:= \mathbf{N}_C q_c^{(\mathbf{v})}, \end{aligned} \tag{2.3}$$

where $\mathbf{I}_3$ is the three order identical matrix, and

$$q_c^{(\mathbf{v})} = (u_1, v_1, w_1, \cdots, u_8, v_8, w_8)^T \in R^{24},$$

are the nodal displacements. Let also

$$\mathbf{U}_I^h := \Big\{ \mathbf{v}_I;\ \mathbf{v}_I|_K \in \text{span}\{1-\xi^2, 1-\eta^2, 1-\zeta^2\}^3 \circ F_K^{-1}, \quad \forall K \in T_h \Big\},$$

be the Wilson's internal displacement subspace, i.e., for $\mathbf{v}_I \in \mathbf{U}_I^h$,

$$\mathbf{v}_I|_K = \Big[(1-\xi^2)\mathbf{I}_3 \quad (1-\eta^2)\mathbf{I}_3 \quad (1-\zeta^2)\mathbf{I}_3\Big] q_I^{(v)} := \mathbf{N}_I q_I^{(\mathbf{v})}, \tag{2.4}$$

where the internal displacements $q_I^{(\mathbf{v})} \in \Re^9$. Then the Wilson's incompatible displacement subspace can be denoted by

$$\mathbf{U}_W^h := \mathbf{U}_1^h \bigoplus \mathbf{U}_I^h,$$

i.e., for $\forall \mathbf{v} \in \mathbf{U}_W^h$,

$$\mathbf{v}|_K = (\mathbf{v}_c + \mathbf{v}_I)|_K = [\mathbf{N}_C \quad \mathbf{N}_I] \left\{ \begin{array}{c} q_c^{(\mathbf{v})} \\ q_I^{(\mathbf{v})} \end{array} \right\}. \tag{2.5}$$

Let

$$\mathbf{V}_1^h := \Big\{ \boldsymbol{\tau} \in \mathbf{V};\ (\tau_{11}, \tau_{22}, \tau_{33})|_K \in \mathrm{span}\{1, \xi, \eta, \zeta, \xi\eta\zeta\}^3 \circ F_K^{-1},$$
$$(\boldsymbol{\tau}_{12}, \boldsymbol{\tau}_{13}, \tau_{23})|_K \in \mathrm{span}\{1, \xi, \eta, \zeta\}^3 \circ F_K^{-1}, \quad \forall K \in T_h \Big\},$$

be the piecewise stress subspace, i.e., stresses $\boldsymbol{\tau} \in \mathbf{V}_1^h$ on K have the form

$$\boldsymbol{\tau}|_K = \left\{ \begin{array}{c} \boldsymbol{\tau}_{11} \\ \boldsymbol{\tau}_{22} \\ \boldsymbol{\tau}_{33} \\ \boldsymbol{\tau}_{12} \\ \boldsymbol{\tau}_{13} \\ \boldsymbol{\tau}_{23} \end{array} \right\} = \left[\begin{array}{cccccccccccccccccc} 1 & 0 & 0 & 0 & 0 & 0 & \xi & 0 & 0 & 0 & 0 & 0 & \eta & 0 & 0 & 0 & 0 & 0 \\ 0 & 1 & 0 & 0 & 0 & 0 & 0 & \xi & 0 & 0 & 0 & 0 & 0 & \eta & 0 & 0 & 0 & 0 \\ 0 & 0 & 1 & 0 & 0 & 0 & 0 & 0 & \xi & 0 & 0 & 0 & 0 & 0 & \eta & 0 & 0 & 0 \\ 0 & 0 & 0 & 1 & 0 & 0 & 0 & 0 & 0 & \xi & 0 & 0 & 0 & 0 & 0 & \eta & 0 & 0 \\ 0 & 0 & 0 & 0 & 1 & 0 & 0 & 0 & 0 & 0 & \xi & 0 & 0 & 0 & 0 & 0 & \eta & 0 \\ 0 & 0 & 0 & 0 & 0 & 1 & 0 & 0 & 0 & 0 & 0 & \xi & 0 & 0 & 0 & 0 & 0 & \eta \end{array} \right.$$
$$\left. \begin{array}{cccccccccc} \zeta & 0 & 0 & 0 & 0 & 0 & \xi\eta\zeta & 0 & 0 \\ 0 & \zeta & 0 & 0 & 0 & 0 & 0 & \xi\eta\zeta & 0 \\ 0 & 0 & \zeta & 0 & 0 & 0 & 0 & 0 & \xi\eta\zeta \\ 0 & 0 & 0 & \zeta & 0 & 0 & 0 & 0 & 0 \\ m0 & 0 & 0 & 0 & \zeta & 0 & 0 & 0 & 0 \\ 0 & 0 & 0 & 0 & 0 & \zeta & 0 & 0 & 0 \end{array} \right] \left\{ \begin{array}{c} \beta_1 \\ \vdots \\ \vdots \\ \vdots \\ \beta_{27} \end{array} \right\} =: \boldsymbol{\Phi}_\beta \beta^{(\boldsymbol{\tau})}. \tag{2.6}$$

Let

$$\mathbf{V}_E^h := \Big\{ \boldsymbol{\tau} \in \mathbf{V}_1^h; \quad \int_K \boldsymbol{\tau} \cdot \epsilon(\mathbf{v}_I) d\Omega = 0, \quad \forall \mathbf{v}_I \in \mathbf{U}_I^h, \quad \forall K \in T_h \Big\},$$

be the energy-compatible stress subspace. Since the energy compatibility condition

$$\int_K \boldsymbol{\tau} \cdot \epsilon(\mathbf{v}_I) d\Omega = 0, \qquad \forall \mathbf{v}_I \in \mathbf{U}_I^h, \tag{2.7}$$

yields 9 linear constraints for the piecewise 27-parameter stresses $\boldsymbol{\tau}$ in (2.6), the energy-compatible stresses in $\mathbf{V}_E^h$ are of $27-9=18$ parameters on K. Due to the complexity of three dimensional case, it's not easy to get the explicit forms of the energy-compatible stresses. But in actual computation we can use them in their implicit forms, as will be discussed in Section 2.2.

Remark 2.1. In fact, one can also give another assumed stress mode which is different from (2.6), say

$$\boldsymbol{\tau}|_K = \begin{Bmatrix} \boldsymbol{\tau}_{11} \\ \boldsymbol{\tau}_{22} \\ \boldsymbol{\tau}_{33} \\ \boldsymbol{\tau}_{12} \\ \boldsymbol{\tau}_{13} \\ \boldsymbol{\tau}_{23} \end{Bmatrix} = \begin{bmatrix} 1 & 0 & 0 & 0 & 0 & 0 & \xi & 0 & 0 & 0 & 0 & 0 & \eta & 0 & 0 & 0 & 0 & 0 \\ 0 & 1 & 0 & 0 & 0 & 0 & 0 & \xi & 0 & 0 & 0 & 0 & 0 & \eta & 0 & 0 & 0 & 0 \\ 0 & 0 & 1 & 0 & 0 & 0 & 0 & 0 & \xi & 0 & 0 & 0 & 0 & 0 & \eta & 0 & 0 & 0 \\ 0 & 0 & 0 & 1 & 0 & 0 & 0 & 0 & 0 & \xi & 0 & 0 & 0 & 0 & 0 & \eta & 0 & 0 \\ 0 & 0 & 0 & 0 & 1 & 0 & 0 & 0 & 0 & 0 & \xi & 0 & 0 & 0 & 0 & 0 & \eta & 0 \\ 0 & 0 & 0 & 0 & 0 & 1 & 0 & 0 & 0 & 0 & 0 & \xi & 0 & 0 & 0 & 0 & 0 & \eta \end{bmatrix}$$
$$\begin{bmatrix} \zeta & 0 & 0 & 0 & 0 & 0 & \eta\zeta & 0 & 0 \\ 0 & \zeta & 0 & 0 & 0 & 0 & 0 & \zeta\xi & 0 \\ 0 & 0 & \zeta & 0 & 0 & 0 & 0 & 0 & \xi\eta \\ 0 & 0 & 0 & \zeta & 0 & 0 & 0 & 0 & 0 \\ 0 & 0 & 0 & 0 & \zeta & 0 & 0 & 0 & 0 \\ 0 & 0 & 0 & 0 & 0 & \zeta & 0 & 0 & 0 \end{bmatrix} \begin{Bmatrix} \beta_1 \\ \vdots \\ \vdots \\ \vdots \\ \beta_{27} \end{Bmatrix}. \tag{2.8}$$

2.2 Element ECH8: element formulations

By taking

$$\mathbf{V}^h = \mathbf{V}_E^h, \quad \text{and} \quad \mathbf{U}^h = \mathbf{U}_1^h,$$

in the variational problem (2.2), i.e., employing the compatible isoparametric trilinear displacements (2.3) and the implicit 18-parameter energy-compatible stress mode, a hybrid stress element named ECH8 is obtained. In other words, ECH8 is based on the following variational principle

$$\Pi_1(\boldsymbol{\sigma}^h, \mathbf{u}_c^h) = \inf_{\mathbf{v}_c \in \mathbf{U}_1^h} \sup_{\boldsymbol{\tau} \in \mathbf{V}_E^h} \Pi_1(\tau, \mathbf{v}_c) = \inf_{\mathbf{v}_c \in \mathbf{U}_1^h} \sup_{\substack{\boldsymbol{\tau} \in \mathbf{V}_1^h \\ \text{satisfying (2.7)}}} \Pi_1(\boldsymbol{\tau}, \mathbf{v}_c), \tag{2.9}$$

where

$$\Pi_1(\boldsymbol{\tau}, \mathbf{v}_c) = \sum_K \Big[-\frac{1}{2} \int_K \boldsymbol{\tau} \cdot \mathbf{D}^{-1} \boldsymbol{\tau} d\Omega + \int_K \boldsymbol{\tau} \cdot \epsilon(\mathbf{v}_c) d\Omega - \oint_{\Gamma_1 \bigcap \partial K} \mathbf{T} \cdot \mathbf{v}_c ds - \int_K \mathbf{f} \cdot \mathbf{v}_c d\Omega \Big].$$

From the second relation in (2.9) we know that the problem can be viewed as a saddle-point problem on $\mathbf{V}_1^h \times \mathbf{U}_1^h$ under the stress constraint (2.7). By introducing the Lagrangian multiplier $\mathbf{u}_I^h \in \mathbf{U}_I^h$ we can easily change this problem into the following constraint-free problem

$$\Pi_2(\boldsymbol{\sigma}^h, \mathbf{u}_c^h, \mathbf{u}_I^h) = \inf_{\mathbf{v} = \mathbf{v}_c + \mathbf{v}_I \in \mathbf{U}_W^h} \sup_{\boldsymbol{\tau} \in \mathbf{V}_1^h} \Pi_2(\tau, \mathbf{v}_c, \mathbf{v}_I), \tag{2.10}$$

where

$$\Pi_2(\boldsymbol{\tau}, \mathbf{v}_c, \mathbf{v}_I) = \sum_K \Big[-\frac{1}{2}\int_K \boldsymbol{\tau}\cdot\mathbf{D}^{-1}\boldsymbol{\tau} d\Omega + \int_K \boldsymbol{\tau}\cdot\epsilon(\mathbf{v}_c+\mathbf{v}_I)d\Omega - \oint_{\Gamma_1\bigcap\partial K}\mathbf{T}\cdot\mathbf{v}_c ds - \int_K \mathbf{f}\cdot\mathbf{v}_c d\Omega\Big].$$

The stationary conditions of (2.10) are known to be: Find

$$(\boldsymbol{\sigma}^h, \mathbf{u}_c^h, \mathbf{u}_I^h) \in \mathbf{V}_1^h \times \mathbf{U}_1^h \times \mathbf{U}_I^h,$$

such that

$$\sum_K \Big\{ \int_K \boldsymbol{\sigma}^h\cdot\mathbf{D}^{-1}\boldsymbol{\tau}\, d\Omega - \int_K \boldsymbol{\tau}\cdot\epsilon(\mathbf{u}_c^h+\mathbf{u}_I^h)\, d\Omega\Big\} = 0, \qquad \forall\boldsymbol{\tau}\in\mathbf{V}_1^h, \quad (2.11)$$

$$\sum_K \int_K \boldsymbol{\sigma}^h\cdot\epsilon(\mathbf{v}_c+\mathbf{v}_I)\, d\Omega = \sum_K \Big\{ \int_K \mathbf{f}\cdot\mathbf{v}_c\, d\Omega + \oint_{\Gamma_1\bigcap\partial K}\mathbf{T}\cdot\mathbf{v}_c\, ds\Big\}, \quad \forall\mathbf{v}_c\in\mathbf{U}_1^h. \quad (2.12)$$

Remark 2.2. When using the stress mode (2.8) instead of (2.6), one can similarly get another energy-compatible hybrid element, which is named $ECH8'$ for convenience.

Remark 2.3. Just like the original incompatible Wilson element(H11), the elements $ECH8$ and $ECH8'$ do not pass the patch test for non-parallelepiped meshes. But as shown in [66], the patch test is not necessary for the convergence of incompatible approximation, and Wilson element gives a convergent solution, provided that the finite meshes satisfied a particular condition, e.g., a bi-section mesh condition. The situation for $ECH8$ and $ECH8'$ is similar.

The element stiffness matrix of ECH8 is derived as follows. From (2.3),(2.4) we have

$$\begin{aligned}\big(\epsilon(\mathbf{v}_c)+\epsilon(\mathbf{v}_I)\big)\big|_K &= \begin{bmatrix} \frac{\partial}{\partial x} & 0 & 0 \\ 0 & \frac{\partial}{\partial y} & 0 \\ 0 & 0 & \frac{\partial}{\partial z} \\ \frac{\partial}{\partial y} & \frac{\partial}{\partial x} & 0 \\ \frac{\partial}{\partial z} & 0 & \frac{\partial}{\partial x} \\ 0 & \frac{\partial}{\partial z} & \frac{\partial}{\partial y} \end{bmatrix} [\mathbf{N}_C \quad \mathbf{N}_I] \begin{Bmatrix} q_c^{(\mathbf{v})} \\ q_I^{(\mathbf{v})} \end{Bmatrix} \\ &=: [\mathbf{B}_C \quad \mathbf{B}_I] \begin{Bmatrix} q_c^{(\mathbf{v})} \\ q_I^{(\mathbf{v})} \end{Bmatrix}. \end{aligned} \quad (2.13)$$

By (2.6) and (2.13), we denote

$$\begin{aligned}\int_K \boldsymbol{\sigma}\cdot D^{-1}\boldsymbol{\tau} d\Omega &= \big(\beta^{(\sigma)}\big)^T \int_{-1}^1\int_{-1}^1\int_{-1}^1 \boldsymbol{\Phi}_\beta^T\mathbf{D}^{-1}\boldsymbol{\Phi}_\beta |J| d\xi d\eta d\zeta \beta^{(\tau)} =: \big(\beta^{(\sigma)}\big)^T\mathbf{H}\beta^{(\tau)}, \\ \int_K \boldsymbol{\tau}\cdot\epsilon(\mathbf{v}_c+\mathbf{v}_I)d\Omega &= \big(\beta^{(\tau)}\big)^T \int_{-1}^1\int_{-1}^1\int_{-1}^1 \boldsymbol{\Phi}_\beta^T[\mathbf{B}_C \quad \mathbf{B}_I]|J| d\xi d\eta d\zeta \begin{Bmatrix} q_c^{(\mathbf{v})} \\ q_I^{(\mathbf{v})} \end{Bmatrix} \\ &=: \big(\beta^{(\tau)}\big)^T[\mathbf{G}_C \quad \mathbf{G}_I] \begin{Bmatrix} q_c^{(\mathbf{v})} \\ q_I^{(\mathbf{v})} \end{Bmatrix}, \end{aligned}$$

$$\int_K \mathbf{f}\cdot\mathbf{v}_c d\Omega + \oint_{\Gamma_1\bigcap\partial K} \mathbf{T}\cdot\mathbf{v}_c ds =: [\mathbf{Q}_c \quad \mathbf{0}] \left\{ \begin{array}{c} q_c^{(\mathbf{v})} \\ q_I^{(\mathbf{v})} \end{array} \right\}.$$

Then it follows from (2.11) that the stress-displacement relation on K is:

$$\beta^{(\sigma^h)} = \mathbf{H^{-1}}[\mathbf{G}_C \quad \mathbf{G}_I] \left\{ \begin{array}{c} q_c^{(\mathbf{u}^h)} \\ q_I^{(\mathbf{u}^h)} \end{array} \right\},$$

Together with Eq. (2.12), we can get the following local system:

$$\left[\begin{array}{cc} \mathbf{G}_C^T\mathbf{H^{-1}}\mathbf{G}_C & \mathbf{G}_C^T\mathbf{H^{-1}}\mathbf{G}_I \\ \mathbf{G}_I^T\mathbf{H^{-1}}\mathbf{G}_C & \mathbf{G}_I^T\mathbf{H^{-1}}\mathbf{G}_I \end{array} \right] \left\{ \begin{array}{c} q_c^{(\mathbf{u}^h)} \\ q_I^{(\mathbf{u}^h)} \end{array} \right\} = \left\{ \begin{array}{c} \mathbf{Q}_c^T \\ \mathbf{0} \end{array} \right\}. \tag{2.14}$$

By following a static condensation process with respect to the internal displacement parameters, the second matrix equation in (2.14) implies

$$q_I^{(\mathbf{u}^h)} = -(\mathbf{G}_I^T\mathbf{H^{-1}}\mathbf{G}_I)^{-1}\mathbf{G}_I^T\mathbf{H^{-1}}\mathbf{G}_C\, q_c^{(\mathbf{u}^h)},$$

Substitute this relation into the first matrix equation (2.14), we then get the element stiffness equation only with respect to the nodal parameters $q_c^{(\mathbf{u}^h)}$:

$$\left(\mathbf{G}_C^T\mathbf{H^{-1}}\mathbf{G}_C - \mathbf{G}_C^T\mathbf{H^{-1}}\mathbf{G}_I(\mathbf{G}_I^T\mathbf{H^{-1}}\mathbf{G}_I)^{-1}\mathbf{G}_I^T\mathbf{H^{-1}}\mathbf{G}_C\right) q_c^{(\mathbf{u^h})} = \mathbf{Q}_c^T. \tag{2.15}$$

2.3 Equivalence to an enhanced strains method

Following the basic idea of [33, 34], in this subsection we will give an equivalent enhanced strains method to the new hybrid stress element *ECH*8.

The equivalent enhanced strains method is based on the following modified Hu-Washizu formulation

$$\begin{aligned}\Pi_3(\mathbf{v}_c,\boldsymbol{\tau},\tilde{\epsilon},\tilde{\epsilon_I}) = \sum_K \Bigg[&-\frac{1}{2}\int_K \tilde{\epsilon}\cdot\mathbf{D}\tilde{\epsilon}d\Omega + \int_K \boldsymbol{\tau}\cdot\Big(\tilde{\epsilon} - \epsilon(\mathbf{v}_c) - \tilde{\epsilon_I}\Big)d\Omega \\ &- \oint_{\Gamma_1\bigcap\partial K}\mathbf{T}\cdot\mathbf{v}_c ds - \int_K \mathbf{f}\cdot\mathbf{v}_c d\Omega\Bigg],\end{aligned}$$

where $\mathbf{v}_c \in \mathbf{U}_c^h$ is the compatible displacements, $\epsilon(\mathbf{v}_c) = (\nabla\mathbf{v}_c + \nabla^T\mathbf{v}_c)/2$ is the strains caused by displacements $\mathbf{v}_c$, $\boldsymbol{\tau} \in \mathbf{V}_1^h$ is the unconstraint stresses,

$$\epsilon \in \mathbf{V}_1^h, \quad \text{and} \quad \epsilon_I \in \mathbf{V}_I^h := \Big\{\epsilon(\mathbf{v}_I) : \mathbf{v}_I \in \mathbf{U}_I^h\Big\},$$

are the independent strains and enhanced strains respectively. The spaces $\mathbf{U}_c^h$, $\mathbf{V}_1^h$, $\mathbf{U}_I^h$ are the same as defined in Section 2.1.

In order to explain its equivalence to $ECH8$, we first give the variational equations of the above enhanced strains method as follows: Find

$$(\boldsymbol{\sigma}^h, \mathbf{u}_c^h, \epsilon, \epsilon_I) \in \mathbf{V}_1^h \times \mathbf{U}_1^h \times \mathbf{V}_1^h \times \mathbf{V}_I^h,$$

such that

$$\sum_K \left\{ \int_K \boldsymbol{\tau} \cdot \left(\epsilon - \epsilon(\mathbf{u}_c^h) - \epsilon_I \right) d\Omega \right\} = 0, \qquad \forall \boldsymbol{\tau} \in \mathbf{V}_1^h, \tag{2.16}$$

$$\sum_K \left\{ \int_K \tilde{\epsilon} \cdot \left(\mathbf{D}\epsilon - \boldsymbol{\sigma}^h \right) d\Omega \right\} = 0, \qquad \forall \tilde{\epsilon} \in \mathbf{V}_1^h, \tag{2.17}$$

$$\sum_K \int_K \boldsymbol{\sigma}^h \cdot \epsilon(\mathbf{v}_c) d\Omega = \sum_K \left\{ \int_K \mathbf{f} \cdot \mathbf{v}_c d\Omega + \oint_{\Gamma_1 \cap \partial K} \mathbf{T} \cdot \mathbf{v}_c ds \right\}, \quad \forall \mathbf{v}_c \in \mathbf{U}_1^h, \tag{2.18}$$

$$\sum_K \left\{ \int_K \boldsymbol{\sigma}^h \cdot \tilde{\epsilon_I} d\Omega \right\} = 0, \qquad \forall \tilde{\epsilon_I} \in \mathbf{V}_I^h. \tag{2.19}$$

We show the equivalence as follows. As we choose the enhanced strains directly from the strains caused by the Wilson bubble displacements, (2.18) and (2.19) are obviously equivalent to (2.12). From (2.17), we know

$$\mathbf{D}\epsilon - \boldsymbol{\sigma}^h = 0, \quad \text{or} \quad \epsilon = \mathbf{D}^{-1}\boldsymbol{\sigma}^h,$$

since

$$\mathbf{D}\epsilon - \boldsymbol{\sigma}^h \in \mathbf{V}_1^h.$$

Substitute this into (2.16), we then get an equation which is the same as (2.11). To sum up, the resultant enhanced strains method and the new hybrid stress element $ECH8$ are equivalent.

Owing to this equivalence, the element $ECH8$ can easily be extended to non-linear problems.

3 Numerical experiments

In this section, some test problems are used to examine numerical performance of the hybrid elements ECH8 and $ECH8'$. The $2 \times 2 \times 2$ Gaussian quadrature is used for all the problems, and it is exact for the computation of ECH8 and $ECH8'$.

Some existing 8-node hexahedral elements are selected for comparison. They are: the isoparametric trilinear element H8, the 3D Wilson element H11, the combined hybrid element CHH(0-1) [56–58], Pian and Tong's hybrid stress hexahedral element $PT18\beta$ [2, 14–16], Sze's element $SS18\beta$ [15] which is the improved version of $PT18\beta$ through admissible matrix formulation, and some famous enhanced strain methods such as SR [31] proposed by Simo and Rifai, HIS [55] proposed by Areias, $3DEAS9$ and $3DEAS30$ [41] proposed by Andelfinger and Ramm. As the element $3DEAS30$ is equivalent to $PT18\beta$, we only need to list the results of $PT18\beta$ in this paper.

It should be mentioned that all the numerical results of $H8$, $H11$, $CHH(0-1)$, $3DEAS9$, as well as of ECH8 and $ECH8'$, are computed by using our codes, while all results of the other elements are from the corresponding references.

3.1 Test for element invariance

The standard test on element invariance is explained by the single-element structure in Fig. 1. Local coordinates frames $\overline{x}-\overline{y}-\overline{z}$ attached to the bases of the structures is shown. The nodal forces acting are defined with respected to the local frames and are parallel to the $\overline{x}-$direction. To test the invariance of the proposed models, the $\overline{x}-\overline{z}$ plane is rotated anti-clockwisely by angles $\pi/8$, $\pi/4$, $3\pi/8$ and $\pi/2$. The computed results for $\overline{x}-$direction displacement of point C are listed in Table 1. The two proposed elements are invariant.

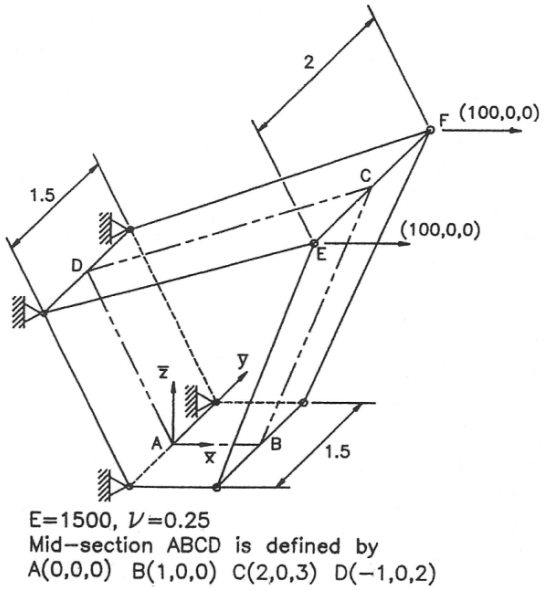

Figure 1: Three-dimensional single element structure for testing element invariance .

3.2 Beam bending

A cantilever beam modeled with five elements is subjected to two different load cases (Fig. 2). The results of every element for the energy Π, the maximum displacement W_A at point A and the normal stress σ_{Bx} at point B are given in Table 2, where $*$ means

Table 1: Computed deflection at point C in the $\overline{x}-$*direction*.

$H8$	$H11$	$3DEAS9$	$PT18\beta$ $3DEAS30$	$CHH(0-1)$	$ECH8$	$ECH8'$
0.4556	0.5737	0.5312	0.5364	0.5775	0.5830	0.5781

Table 2: Cantilever beam with five irregular elements.

	Case 1			Case 2		
Element	W_A	σ_{Bx}	$\Pi(\times 10^4)$	W_A	σ_{Bx}	$\Pi(\times 10^4)$
$H8$	44.4	-1736.3	1.64	49.3	-2415.3	1.47
$H11$	98.3	-3037.9	3.86	100.2	-4224.8	3.01
$H11^*$	89.7	-2892.1	3.53	92.2	-4020.5	2.77
$CHH(0-1)$	98.3	-3002.4	3.86	100.3	-4159.1	3.01
$CHH(0-1)^*$	93.8	-2927.2	3.69	96.1	-4054.0	2.89
$3DEAS9$	95.7	-3000.3	3.70	97.8	-4131.6	2.94
$PT18\beta, 3DEAS30$	98.3	-3002.5	3.86	100.3	-4159.3	3.01
$SS18\beta$	98.3	-3002.3	3.86	100.3	-4159.1	3.01
HIS	95.9	—	—	97.8	—	—
$ECH8$	98.4	-3001.5	3.87	100.4	-4158.7	3.02
$ECH8'$	98.3	-3002.3	3.87	100.3	-4159.2	3.01
Exact	100.0	-3000.0	4.00	102.6	-4050	3.08

the use of $3 \times 3 \times 3$ Gaussian quadrature. We can see that the proposed elements ECH8 and $ECH8'$ give almost the best results.

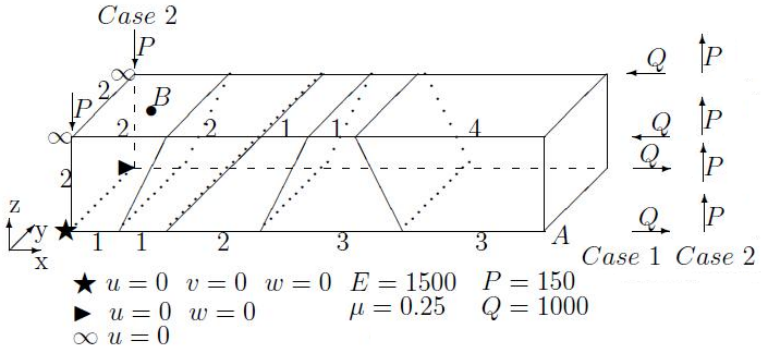

Figure 2: Finite element mesh for cantilever beam problem.

3.3 Beam bending: sensitivity to mesh distortion

In this standard test, a beam under bending is only analyzed with two hexahedron elements (Fig. 3). The distortion degree of element is measured by parameter e. The results of every element for the maximum displacement W_A at point A are given in Table 3. The elements ECH8 and $ECH8'$ behave well.

3.4 MacNeal-Harder's slender cantilever beams

A slender cantilever beam proposed by MacNeal and Harder [62] is used to test the scheme accuracy under the influence of geometrical parameters of problem such as aspect ratio. In Fig. 4, a straight beam of dimension $6 \times 0.2 \times 0.1$ is analyzed with six

Table 3: The results of W_A for mesh distortion.

Element	e=0.5	e=1	e=2	e=3	e=4	e=4.9	Exact
$H8$	20.8	13.9	9.6	8.2	7.1	6.1	
$H11$	92.6	85.9	91.8	101.8	110.1	116.3	
$CHH(0-1)$	92.7	85.9	92.0	102.2	110.6	116.8	
$3DEAS9$	82.9	65.8	60.9	64.0	65.0	62.7	100.0
$PT18\beta, 3DEAS30$	88.6	74.3	57.0	50.3	46.6	42.3	
$SS18\beta$	88.8	79.9	68.0	63.7	61.4	60.6	
$ECH8$	93.2	87.0	93.1	103.1	111.4	117.6	
$ECH8'$	92.9	86.1	92.3	102.6	111.1	117.5	

Table 4: The tip deflections and energy for slender cantilever beam.

Element	H8	H11	$3DEAS9$	$PT18\beta$ $3DEAS30$	$SS18\beta$	ECH8	$ECH8'$
W_A	0.0109	0.4204	0.4204	0.4233	0.4235	0.4291	0.4237
Π	-0.0054	-0.2102	-0.2102	-0.2112	-0.2117	-0.2145	-0.2119

regular hexahedron elements. An out-of-plain end shear is acting on the beam. The results of tip deflection W_A in the direction of loading and the energy Π are listed in Table 4 and the reference is $W_A = 0.4321, \Pi = -0.2159$. We can see that ECH8 gives the best results.

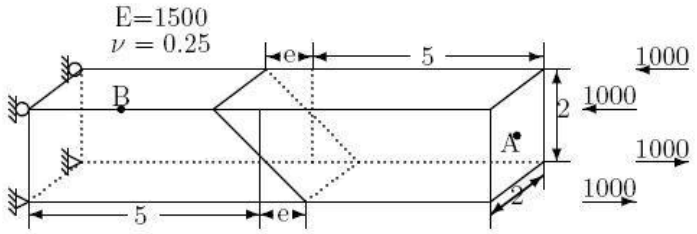

Figure 3: Cantilever beam for mesh distortion test.

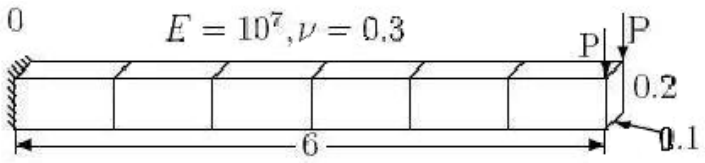

Figure 4: Straight-beam.

3.5 Poisson's ratio locking free test

This example is chosen for testing the behavior of elements under the incompressible limit condition (Poisson's ratio varies from 0.3 to 0.49999) [19]. The cantilever beam are

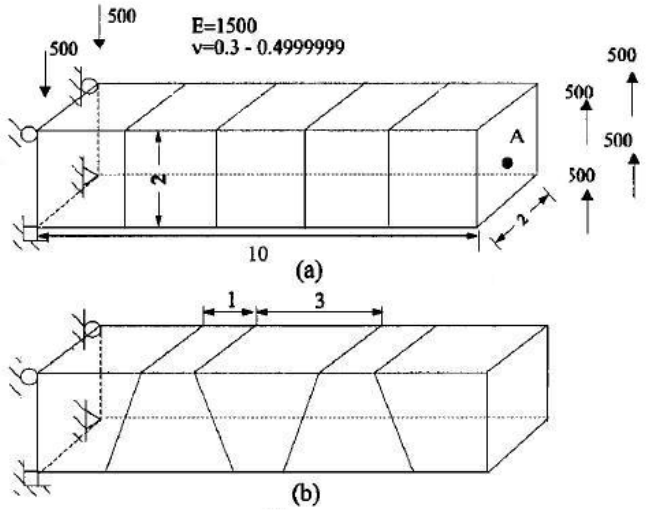

Figure 5: Volumetric test for a cantilever beam.

analyzed with five cubic elements in Fig. 5(a) and five irregular elements in (b). The results of every element except $SS18\beta$ for the maximum displacement W_A at point A, the energy Π and the normal stress σ_{Bx} at point B are given in Tables 5 to 7 and Table 8 to 10, respectively. The elements ECH8 and $ECH8'$ are uniformly accurate.

3.6 Convergence test for solid

A clamped tapered cantilever with varying thickness is considered. This problem was modified from Cook's membrane [51] to test the accuracy of hexahedron elements (see Fig. 6). The results for the tip deflection at point A of mesh $4 \times 4 \times 1$ and $8 \times 8 \times 2$ are

Table 5: The displacement of cubic elements for Poisson's ratio test.

ν	$H8$	$H11$	$3DEAS9$	$PT18\beta$ $3DEAS30$	$ECH8$	$ECH8'$	Exact
0.3	222.9	338.1	338.1	345.4	338.7	338.4	
0.4	204.4	338.1	338.1	345.8	339.3	338.9	342
0.49	169.7	332.5	332.5	346.1	339.9	339.2	
0.49999	135.1	320.0	320.0	346.3	340.0	339.3	

Table 6: The energy $\Pi(\times(-10^5))$ of cubic elements for Poisson's ratio test.

ν	$H8$	$H11$	$3DEAS9$	$PT18\beta$ $3DEAS30$	$ECH8$	$ECH8'$	Exact
0.3	2.23	3.38	3.38	3.45	3.39	3.38	
0.4	2.04	3.38	3.38	3.45	3.39	3.39	3.42
0.49	1.69	3.32	3.32	3.46	3.40	3.39	
0.49999	1.35	3.20	3.20	3.46	3.40	3.39	

Table 7: The stress $\Pi(\times 10^4)$ of cubic elements for Poisson's ratio test.

ν	$H8$	$H11$	$3DEAS9$	$PT18\beta$ $3DEAS30$	$ECH8$	$ECH8'$	Exact
0.3	-1.01	-1.82	-1.82	-1.35	-1.35	-1.35	
0.4	-1.07	-2.93	-2.93	-1.35	-1.35	-1.35	-1.35
0.49	-1.14	-25.06	-25.06	-1.35	-1.35	-1.35	
0.49999	-1.22	-27492	-27492	-1.35	-1.35	-1.35	

shown in Table 11. The elements ECH8 and $ECH8'$ give best convergent results.

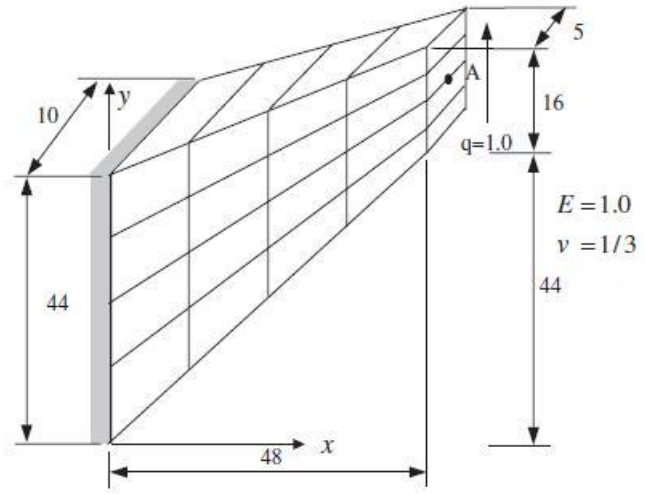

Figure 6: Solid convergence test.

Table 8: The displacement of irregular elements for Poisson's ratio test.

ν	$H8$	$H11$	$3DEAS9$	$PT18\beta$ $3DEAS30$	$ECH8$	$ECH8'$	Exact
0.3	189.6	301.3	266.6	284.2	302.7	302.4	
0.4	178.5	298.7	266.7	284.5	301.0	300.5	342
0.49	157.4	291.8	263.0	283.9	298.6	297.8	
0.49999	150.5	288.5	260.9	283.1	298.2	297.4	

Table 9: The energy $\Pi\big(\times(-10^5)\big)$ of cubic elements for Poisson's ratio test.

ν	$H8$	$H11$	$3DEAS9$	$PT18\beta$ $3DEAS30$	$ECH8$	$ECH8'$	Exact
0.3	1.89	3.04	2.70	2.87	3.05	3.05	
0.4	1.78	3.01	2.69	2.88	3.03	3.03	3.42
0.49	1.56	2.94	2.65	2.85	3.01	3.00	
0.49999	1.49	2.91	2.63	2.83	3.01	3.00	

Table 10: The stress $\Pi(\times 10^4)$ of cubic elements for Poisson's ratio test.

ν	$H8$	$H11$	$3DEAS9$	$PT18\beta$ $3DEAS30$	$ECH8$	$ECH8'$	Exact
0.3	-0.80	-1.61	-1.55	-1.33	-1.34	-1.34	
0.4	-0.76	-2.68	-2.53	-1.33	-1.34	-1.34	-1.35
0.49	0.4683	-23.87	-21.65	-1.32	-1.33	-1.33	
0.49999	1298.5	-24237	-21576	-1.32	-1.33	-1.33	

Table 11: Solid convergence test.

Elements	$H8$	$H11$	$3DEAS9$	$CHH(0-1)$	$ECH8$	$ECH8'$
$4\times4\times1$	365.73	499.39	477.13	499.67	500.19	499.75
$8\times8\times2$	460.23	507.54	501.73	507.58	507.63	507.59
Exact			508.11			

3.7 Simply supported square plate subjected to uniform loading

A simply supported square plate with varies range of thickness/ span ratio (t/L) subjected to a uniform load (Fig. 7) is used to test shear locking phenomenon of the hexahedral elements. Owing to symmetry, only one-quarter of the plate is analyzed by $N \times N$ elements. The results of the central deflection under different thickness/ span ratio are given from Table 12 to Table 15. From Table 12 we can see that ECH8 and $ECH8'$ are quite accurate when $t/L \geq 10^{-4}$.

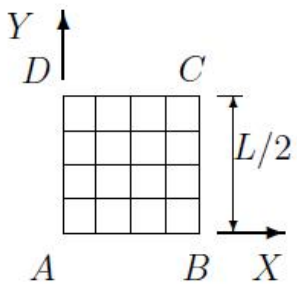

$E = 10920;\ \nu = 0.3;$
$t = 0.1,\ 2,\ L = 10;\ L/t = 100, L/t = 5$
uniform loading: $q = 1$
Boundary conditions on BC & CD:
For clamped plate: $\omega = \beta_s = \beta_n = 0$
For SS2 plate: $\omega = \beta_s = 0$
Symmetry conditions:
$\beta_x = 0$ on AD and $\beta_y = 0$ on AB

Figure 7: Quadrant of a square plate: geometry and 4×4 mesh.

3.8 One-quarter of circle plate

In this test, one-quarter of a clamped circle plate is used to demonstrate the versatility of the proposed elements. Three meshes of 3, 12 and 48 elements are considered (Fig. 8). The results of the central deflection are listed in Table 16. We can see that ECH8 and $ECH8'$ behave almost the best.

Table 12: Central deflection for simply supported square plate with a uniform load discretized into 6×6 in different thickness/ span ratios.

t/L	0.2	0.01	0.001	10^{-4}	10^{-5}
$H8$	393.6	30.69	0.337	3.4e-3	3.4e-5
$H11$	475.5	3579.1	51.15	0.584	5.9e-3
$3DEAS9$	470.9	377.4	48.14	0.545	5.5e-3
$CHH(0-1)$	476.5	392.6	90.90	1.167	0.012
$ECH8'$	476.4	406.0	405.8	401.5	31.30
$ECH8$	477.4	407.1	406.9	409.9	24.41
$Refence$	490.8	406.4	406.2	406.2	406.2

Table 13: Simply supported square plate (uniform load, $t/L = 0.2$).

N	2	4	6	10	16
$H8$	338.4	383.8	393.6	398.8	400.6
$H11$	462.5	474.2	475.5	476.1	476.3
$3DEAS9$	457.9	469.7	470.9	471.5	471.6
$CHH(0-1)$	473.9	476.5	476.5	476.4	476.4
$ECH8'$	475.6	476.3	476.4	476.4	476.4
$ECH8$	486.1	478.7	477.4	476.8	476.5
$Reference$			490.8		

3.9 Morley's skew plate

Fig. 9 shows the mesh generated for the Morley's simply supported rhombic plate [61] with skew angle $\Theta = 30^\circ$, subject to a uniform load. The results of central deflection are given in Table 17. The element ECH8 behaves the best.

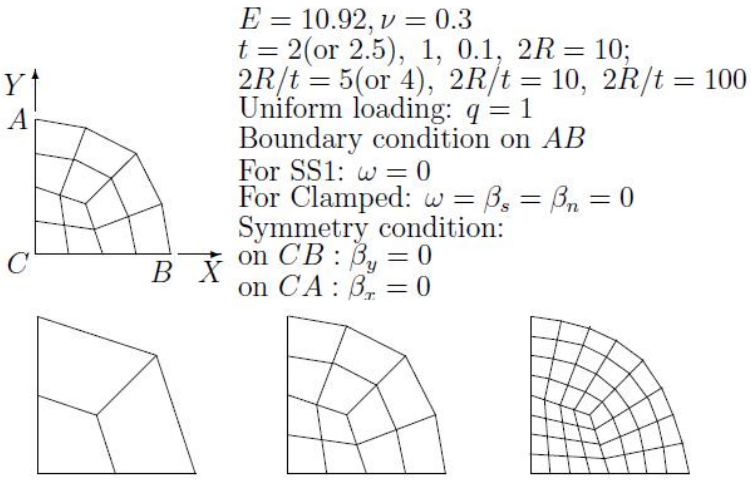

Figure 8: Three meshes for quadrant of a circular plate.

Table 14: Simply supported square plate (uniform load, $t/L = 0.01$).

N	2	4	6	10	16
$H8$	3.719	14.38	30.69	73.22	139.5
$H11$	56.78	298.5	379.1	402.4	405.7
$CHH(0-1)$	99.73	344.7	392.6	404.5	406.1
$3DEAS9$	53.52	293.1	377.4	402.2	405.7
$PT18\beta, 3DEAS30$	401.3	405.1	405.6	406.1	406.3
$SS18\beta$	421.8	413.3	408.7	407.2	406.6
EAS[34]	398.9	404.9	—	—	406.3
HIS	432.0	412.9	—	—	410.9
SR	397.1	404.4	—	—	406.3
$ECH8'$	402.0	405.5	406.0	406.3	406.4
$ECH8$	412.5	407.9	407.1	406.6	406.5
$Reference$			406.4		

Table 15: Simply supported square plate (uniform load, $t/L = 0.001$).

N	2	4	6	10	16
$H8$	0.038	0.150	0.337	0.935	2.383
$H11$	0.662	11.09	51.15	214.6	357.6
$CHH(0-1)$	1.319	21.60	90.90	281.0	380.4
$3DEAS9$	0.617	10.37	48.14	207.7	354.6
$PT18\beta, 3DEAS30$	401.4	405.0	405.5	405.9	406.1
$SS18\beta$	421.2	412.6	408.1	406.8	406.4
$ECH8'$	401.8	405.3	405.8	406.1	406.2
$ECH8$	412.3	407.7	406.9	406.5	406.3
$Reference$			406.2		

3.10 Scordelis roof

In Fig. 10, a 80° cylindrical roof is supported on two rigid diaphragms and subjected to a gravity loading g of intensity 90 unit per unit midsurface area. Owing to symmetry, only a quarter of the roof is modeled. The vertical displacement at the midpoint A of the free-hanging edge is normalized in Table 18. This is a widely employed bench-

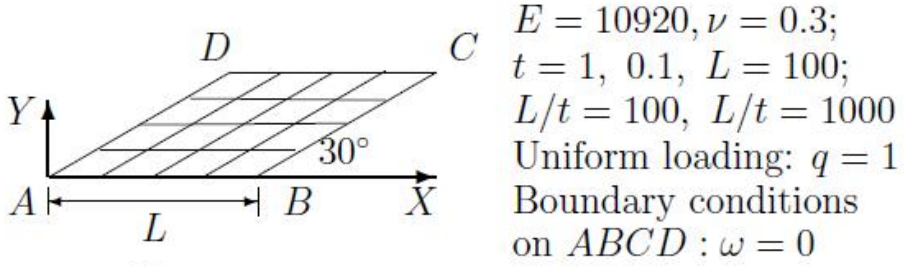

Figure 9: Morley's acute skew plate: geometry and 4×4 mesh.

Table 16: Central deflection for clamped circle plate.

t/R	0.2			0.02		
n	3	12	48	3	12	48
$H8$	3.4722	6.5017	8.4755	48.501	176.60	647.14
$H11$	9.4704	10.879	11.169	1418.4	6469.6	9369.0
$CHH(0-1)$	9.902	10.985	11.192	2288.5	7636.0	9546.3
$3DEAS9$	7.688	10.338	11.029	1134.4	6021.0	9233.4
$PT18\beta, 3DEAS30$	5.972	10.038	11.155	5058.1	8501.9	9617.2
$SS18\beta$	9.322	10.384	11.185	5865.9	9118.2	9618.3
EAS[34]	—	—	—	—	9163.3	9686.6
HIS	—	—	—	3081.8	8002.9	9578.0
SR	—	—	—	—	9079.8	9613.8
$ECH8'$	10.226	11.036	11.200	6339.5	9417.2	9722.3
$ECH8$	10.411	11.092	11.214	6430.0	9473.6	9736.6
$Refence$		11.551			9783.5	

Table 17: Central deflection for the Morley's skew (30°) plate.

t/L	0.01			0.001		
n	4	8	16	4	8	16
$H8$	0.009	0.029	0.075	9.5e-5	3.8e-4	1.5e-3
$H11$	0.132	0.277	0.364	0.003	0.038	0.178
$CHH(0-1)$	0.172	0.302	0.377	0.005	0.064	0.210
HIS	0.419	0.410	0.405	—	—	—
$3DEAS9$	0.132	0.277	0.364	0.003	0.038	0.178
$SS18\beta$	—	—	—	0.415	0.393	0.396
$ECH8'$	0.391	0.400	0.402	0.365	0.383	0.401
$ECH8$	0.437	0.435	0.421	0.436	0.434	0.419
Kirchhoff solution[60]					0.408	
3D solution[61]		0.424				

Table 18: Normalized deflection for Scordelis-Loroof.

$Mesh$	2×2	4×4	6×6	8×8
$H8$	0.0038	0.0117	0.0209	0.0314
$H11$	0.0311	0.1415	0.2444	0.2836
$CHH(0-1)$	0.0460	0.1922	0.2736	0.2957
$3DEAS9$	0.0329	0.1411	0.2441	0.2835
$PT18\beta, 3DEAS30$	0.4677	0.3291	0.3117	0.3092
$SS18\beta$	0.4702	0.3274	0.3145	0.3108
HIS	0.4194	0.3175	0.3114	0.3089
$ECH8'$	0.1953	0.3015	0.3070	0.3073
$ECH8$	0.4666	0.3225	0.3118	0.3090
$Reference$		0.3086		

mark problem for evaluating new shell elements and most of the plate/ shell elements overestimate the deflection when the mesh is coarse. From Table 18 we can see that ECH8 and $ECH8'$ give very accurate results.

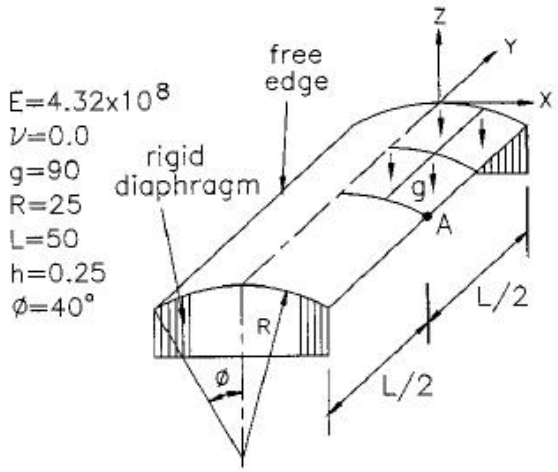

Figure 10: Scordelis-Lo's Roof loaded by its own weight.

4 Conclusions

For three-dimensional elasticity, the energy-compatibility condition has been shown to be an efficient stress-optimization condition for the construction of high performance low order hybrid stress hexahedron elements based on the Hellinger-Reissner variational principle. By following this condition, a robust 8-node hexahedral element formulation has been derived. Due to elimination of stress parameters at the element level, the proposed elements are of almost the same computational cost as that of H8. The equivalence to an enhanced strains method has been established. This ensures the convenience of the extension of the proposed hybrid stress method to general nonlinear problems. Numerical tests have shown that the new method is of high accuracy at coarse meshes, insensitive to mesh distortions and free from volume locking in the analysis of beams, plates and shells.

Acknowledgments

This work was supported in part by the Natural Science Foundation of China (10771150), the National Basic Research Program of China (2005CB321701), and the Program for New Century Excellent Talents in University (NCET-07-0584).

References

[1] T. H. H. PIAN AND K. SUMIHARA, *Rational approach for assumed stress finite elements*, Int. J. Numer. Meth. Engng., 20 (1984), pp. 1685-1695.

[2] T. H. H. PIAN AND P. TONG, *Relations between incompatible displacement model and hybrid stress model*, Int. J. Numer. Meth. Engng., 22 (1986), pp. 173-181.

[3] T. H. H. PIAN AND C. C. WU, *A rational approach for choosing stress terms for hybrid finite element formulation*, Int. J. Numer. Meth. Engng., 26 (1988), pp. 2331-2343.
[4] K. Y. YUAN AND T. H. H. PIAN, *New strategy for assumed stress for 4-node hybrid stress membrane element*, Int. J. Numer. Meth. Engng., 36 (1993), pp. 1747-1763.
[5] K. Y. YUAN, J. C. WEN AND T. H. H. PIAN, *A unified theory for formulation of hybrid stess membrane elements*, Int. J. Numer. Meth. Engng., 37 (1994), pp. 457-474.
[6] T. H. H. PIAN, *State-of-art development of hybrid/ mixed finite element method*, Finite. Elem. Anal. Des., 21 (1995), pp. 5-20.
[7] W. J. CHEN AND Y. K. CHEUNG, *A new approach for the hybrid element method*, Int. J. Numer. Meth. Engng., 24 (1987), pp. 1697-1709.
[8] W. J. CHEN AND Y. K. CHEUNG, *Robust refined quadrilateral plane element*, Int. J. Numer. Meth. Engng., 38 (1995), pp. 649-666.
[9] M. C. BOUZEGHOUB AND M. J. GUNN, *On stress interpolation for hybrid models*, Int. J. Numer. Meth. Engng., 37 (1994), pp. 895-904.
[10] C. C. WU AND Y. K. CHEUNG, *On optimization approaches of hybrid stress elements*, Finite. Elem. Anal. Des., 21 (1995), pp. 111-128.
[11] R. L. SPILKER AND S. P. SINGH, *Three-dimensional hybrid-stress isoparametric quadratic displacement element*, Int. J. Numer. Meth. Engng., 18 (1982), pp. 445-465.
[12] E. F. PUNCH AND S. N. ATLURI, *Application of isoparametric three dimensional hybrid stress finite elements with least-order stress field,*. Comput. Struct., 19 (1984), pp. 409-430.
[13] E. F. PUNCH AND S. N. ATLURI, *Development and testing of stable, invariant, isoparametric curvilinear 2- and 3-D hybrid-stress elements*, Comp. Methods. Appl. Mech. Eng., 47 (1984), pp. 331-356.
[14] K. Y. SZE, *Efficient formulation of robust hybrid elements using orthogonal stress/ strain interpolants and admissible matrix formulation*, Int. J. Numer. Methods. Engng., 35 (1992), pp. 1-20.
[15] K. Y. SZE, *Hybrid hexahedral element for solids,plates,shells and beams by selective scaling*, Int. J. Numer. Methods. Engng., 36 (1993), pp. 1519-1540.
[16] K. Y. SZE, *Admissible matrix formulation-from orthobonal approach to explicit hybrid stabilization*, Finite. Elem. Anal. Des., 24 (1996), pp. 1-30.
[17] K. Y. SZE AND H. FAN, *An economical assumed stress brick element and its application*, Finite. Elem. Anal. Des., 21 (1996), pp. 179-200.
[18] K. Y. SZE, C. L. CHOW AND W. J. CHEN, *A rational formulation of isoparametric hybrid stress elements for three-dimensional stress analysis*, Finite. Elem. Anal. Des., 7 (1990), pp. 61-72.
[19] S. T. YEO AND B. C. LEE, *New stress assumption for hybrid stress elements and refined four-node plane and eight-node brick elements*, Int. J. Numer. Methods. Engng., 40 (1997), pp. 2933-2952.
[20] J. P. M. D. ALMEIDA AND O. J. B. A. PEREIRA, *A set of hybrid equilibrium finite element methods for the analysis of three-dimensional solids*, Int. J. Numer. Meth. Engng., 39 (1996), pp. 2789-2802.
[21] Y. F. DONG AND J. A. T. D. FREITAS, *An efficient eight-node incompatible solid element with stress interpolation*, Comp. Struct., 44 (1992), pp. 773-781.
[22] T. X. ZHOU AND X. P. XIE, *A unified analysis for stress/ strain hybrid methods of high performance*, Comput. Methods. Appl. Mech. Engng., 191 (2002), pp. 4619-4640.
[23] X. P. XIE AND T. X. ZHOU, *Optimization of stress modes by energy compatibility for 4-node hybrid quadrilaterals*, Int. J. Numer. Meth. Engng., 59 (2004), pp. 293-313.
[24] X. P. XIE, *An accurate hybrid macro-element with linear displacements*, Comm. Numer. Meth. Engng., 21 (2005), pp. 1-12.

[25] X. P. XIE AND T. X. ZHOU, *Accurate 4-node quadrilateral elements with a new version of energy-compatible stress mode*, Commun. Numer. Meth. Engng., in press.
[26] T. J. R. HUGHES, *Generalization of selective integration procedures to anisotropic and nonlinear media*, Int. J. Numer. Meth. Engng., 15 (1980), pp, 1413-1418.
[27] D. P. FLANAGAN AND T. BELYTSCHKO, *A uniform strain hexahedron and quadrilateral with orthogonal hourglass control*, Int. J. Numer. Meth. Engng., 17 (1981), pp. 679-706.
[28] E. P. KASPER AND R. L. TAYLOR, *A mixed-enhanced strain method - part I: Geometrically linear problems*, Comp. Struct., 75 (2000), pp. 237-250.
[29] J. C. SIMO, R. L. TAYLOR AND K. S. PISTER, *Variational and projection methods for the volume constraint in finite deformation elasto-plasticity*, Comput. Meth. Appl. Mech. Engng., 51 (1985), pp. 177-208.
[30] Y. K. CHEUNG AND W. CHEN, *Isoparametric hybrid hexahedral elements for three dimensional stress analysis*, Int. J. Numer. Meth. Engng., 26 (1988), pp. 677-693.
[31] J. C. SIMO AND M. S. RIFAI, *A class of assumed strain methods and the method of incompatible modes*, Int. J. Numer. Meth. Engng., 29 (1990), pp. 1595-1638.
[32] R. PILTNER AND R. L TAYLOR, *A quadrilateral mixed finite element with two enhanced strain modes*, Int. J. Numer. Meth. Engng., 38 (1995), pp. 1783-1808.
[33] R. PILTNER AND R. L. TAYLOR, *A systematic construction of B-bar functions for linear and non-linear mixed-enhanced finite elements for plane elasticity problems*, Int. J. Numer. Meth. Engng., 44 (1999), pp. 615-639.
[34] R. PILTNER, *An alternative version of the Pian-Sumihara element with a simple extention to non-linear problems*, Comput. Mech., 26 (2000), pp. 483-489.
[35] R. PILTNER AND D. S. JOSEPH, *A mixed finite element for plate brnding with eight enhanced strain modes*, Commun. Numer. Meth. Engng., 17 (2001), pp. 443-454.
[36] B. D. REDDY AND J. C. SIMO, *Stability and convergence of a class of enhanced strain methods*, SIAM. J. Numer. Anal., 32 (1995), pp. 1705-1728.
[37] J. C. SIMO AND F. ARMERO, *Geometrically non-linear enhanced strain mixed methods and the method of incompatible modes*, Int. J. Numer. Meth. Engng., 33 (1992), pp. 1413-1449.
[38] W. J. CHEN AND Y. K. CHEUNG, *Three-dimensional 8-node and 20-node refined hybrid isoparametric elements*, Int. J. Numer. Meth. Engng., 35 (1992), pp. 1871 - 1889.
[39] J. C. SIMO, D. D. FOX AND M. S. RIFAI, *On a stress resultant geometrically exact shell model, Part II: The linear theory; computational aspects*, Comput. Meth. Appl. Mech. Engng., 73 (1989), pp. 53-92.
[40] J. C. SIMO, F. ARMERO AND R. L. TAYLOR, *Improved versions of assumed enhanced strain tri-linear elements for 3D finite deformation problems*, Comput. Meth. Appl. Mech. Engng., 110 (1993), pp. 359-386.
[41] U. ANDELFINGER AND E. RAMM, *EAS-elements for two-dimensional, three-dimensional, plate and shell structures and their equivalence to HR-elements*, Int. J. Numer. Meth. Engng., 36 (1993), pp. 1311-1337.
[42] T. BELYTSCHKO AND L. P. BINDEMAN, *Assumed strain stabilization of the eight node hexahedral*, Comput. Meth. Appl. Mech. Engng., 105 (1993), pp. 225-260.
[43] J. KORELC AND P. WRIGGERS, *Efficient enhanced strain element formulation for 2D and 3D problems*, In Advances in Finite Element Technology. Wiberg NE (ed.). CIMNE: Barcelona, Spain, 1995, pp. 22-46.
[44] Y. Y. ZHU AND S. CESCOTTO, *Unified and mixed formulation of the 8-node hexahedral elements by assumed strain method*, Comput. Meth. Appl. Mech. Engng., 129 (1996), pp. 177-209.
[45] D. ROEHL AND E. RAMM, *Large elasto-plastic finite element analysis of solids and shells with the enhanced assumed strain concept*, Int. J. Solids. Struct., 33 (1996), pp. 3215-3237.

[46] S. L. WEISSMAN, *High-accuracy low-order three-dimensional brick elements*, Int. J. Numer. Meth. Engng., 39 (1996), pp. 2337-2361.
[47] S. GLASER AND F. ARMERO, *On the formulation of enhanced strain finite elements in finite deformations*, Engng. Comput., 14 (1997), pp. 759-791.
[48] Y. T. CHEN AND H. K. STOLARSKI, *Extrapolated fields in the formulation of the assumed strain elements, Part II: Threedimensional problems*, Comput. Meth. Appl. Mech. Engng., 154 (1998), pp. 1-29.
[49] W. K. LIU, Y. GUO AND T. BELYTSCHKO, *A multiple-quadrature eight-node hexahedral finite element for large deformation elastoplastic analysis*, Comput. Meth. Appl. Mech. Engng., 154 (1998), pp. 69-132.
[50] M. A. PUSO, *A highly efficient enhanced assumed strain physically stabilized hexahedral element*, Int. J. Numer. Meth. Engng., 49 (2000), pp. 1029-1064.
[51] E. A. DE SOUZA NETO, D. PERIC, M. DUTKO AND D. R. J. OWEN, *Design of simple low order finite elements for large strain analysis of nearly incompressible solids*, Int. J. Solids. Struct., 33 (1996), pp. 3277-3296.
[52] S. REESE, M. KUSSNER AND B. D. REDDY, *A new stabilization technique for finite elements in non-linear elasticity*, Int. J. Numer. Meth. Engng., 44 (1999), pp. 1617-1652.
[53] S. REESE, P. WRIGGERS AND B.D. REDDY, *A new locking-free brick element technique for large deformation problems in elasticity*, Comput. struct., 75 (2000), pp. 291-304.
[54] Y. P. CAO, N. HU, J. LU, H. FUKUNAGA AND Z. H. YAO, *A 3D brick element based on Hu-washizu variational principle for mesh distortion*, Int. J. Numer. Meth. Engng., 53 (2002), pp. 529-548.
[55] P. M. A. AREIAS, J. M. A. CéSAR DE Sá, C. A. CONCEIÇãO ANTóNIO AND A.A. FERNANDES, *Analysis of 3D problems using a new enhanced strain hexahedral element*, Int. J. Numer. Meth. Engng., 58 (2003), pp. 1637–1682.
[56] T. X. ZHOU AND Y. F. NIE, *A combined hybrid approach to finite element schemes of high performance*, Int. J. Numer. Meth. Engng., 51 (2001), pp. 181-202.
[57] T. X. ZHOU, *Stabilized hybrid finite element methods based on combination of saddle point principles of elasticity problem*, Math. Comp., 72 (2003), pp. 1655-1673.
[58] Y. F. NIE AND T. X. ZHOU, *8-node hexahedron combined hybrid el- ement with high performances. (in Chinese)*, J. Numer. Meth. Comput. Appl., 3 (2003), pp. 231-240.
[59] T. X. ZHOU AND X. P. XIE, *Zero energy-error mechanism of the combined hybrid method and improvement of Allman's membrane element with drilling d.o.f.s*, Comm. Numer. Meth. Engng., 20 (2004), pp. 241-250.
[60] R. L. TAYLOR, P. J. BERESFORD AND E. L. WILSON, *A nonconforming element for stress analysis*, Int. J. Numer. Meth. Engng., 10 (1976), pp. 1211-1219.
[61] M. J. LOIKKANEN AND B. M. IRONS, *A 8-node brick finite element*, Int. J. Numer. Meth. Engng., 20 (1983), pp. 523-528.
[62] R. H. MACNEAL AND R. L. HARDER, *A proposed set of problems to test finite element accuracy*, Finite. Elem. Anal. Des., 1 (1985), pp. 13-20.
[63] L. S. D. MORLEY, Skew Plates and Structures, Pergamon Press: Oxford, 1963.
[64] I. BABUSKA AND T. SCAPOLLA, *Benchmark computation and performance evaluation for a rhombic plate bending problem*, Inter. J. Numer. Meth. Engrg., 28 (1989), pp. 155-179.
[65] C. K. CHOI, T. Y. LEE AND K. Y. CHUNG, *Direct modification for non-conforming elements with drilling DOF*, Int. J. Numer. Meth. Engng., 55 (2002), pp. 1463-1476.
[66] Z.C. SHI, *A convergence condition for the quadrilateral Wilson element*, Numer. Math., 44 (1984), pp. 349-361.